# CHAPTER 22

# SEASONALITY EXTRACTION FROM TIME-SERIES OF SATELLITE SENSOR DATA

[1,2]Per Jönsson and [3]Lars Eklundh

[1]*Division of Mathematics, Natural Sciences and Language*
*Malmö University, Malmö, Sweden*
[2]*Department of Physics, Lund University, Lund, Sweden*
*E-mail: Per.Jonsson@ts.mah.se*
[3]*Department of Physical Geography and Ecosystems Analysis*
*Lund University, Lund, Sweden*
*E-mail: Lars.Eklundh@nateko.lu.se*

Two methods for processing time-series of satellite sensor data are presented. The first method is based on an adaptive Savitzky-Golay filter, and the second on non-linear least-squares fits to asymmetric Gaussian model functions. Both methods incorporate qualitative information on cloud contamination from ancillary datasets. The resulting smooth curves are used for extracting phenological parameters related to the growing seasons. The methods are applied to NASA/NOAA Pathfinder AVHRR Land Normalized Difference Vegetation Index (NDVI) data over Africa giving spatially coherent images of phenological parameters such as beginnings and ends of growing seasons, seasonally integrated NDVI, seasonal amplitudes etc. The results indicate that the two methods complement each other and that they may be suitable in different areas depending on the behavior of the NDVI signal.

## 1. Introduction

To extract seasonality information it is necessary to generate smooth time-series from noisy satellite sensor data. This can be achieved by applying simple filters or by function fitting. A commonly used filtering method, BISE[1], is easy to implement, but makes the usually erroneous assumption that all noise is negatively biased. Methods based on e.g. Fourier series[2,3] or on least-squares fits to sinusoidal functions[4–6] perform well if the shape of the time-profile is characterized by a well-defined annual cycle of growth and decline, but may fail when the time-profile is more ambiguous. Although most vegetation-covered areas are characterized by a clear annual growth and decline pattern, the shape of the time-profile may vary significantly between different bio-climatic zones. In some areas the time-profile is simple, allowing for the fitting of sinusoidal or bell-shaped functions. In other areas, particularly arid areas where the growing season is very short, the time-profile

has quite a different shape, and simple functions are often unable to describe the data. For this reason it is necessary to consider methods that are based on different assumptions regarding the shape of the annual time-profile. We present and test two new methods; adaptive Savitzky-Golay filtering with no prior assumptions on the time-profile, and non-linear least-squares fits to asymmetric Gaussians with the rather weak assumption that the growing season is characterized by a well-defined increase up to a peak level from which it declines until its end.

## 2. Data

The new methods are tested with the NASA/NOAA Pathfinder AVHRR Land (PAL) 8 km by 8 km database[7,8]. These data are well documented and have been used for global and regional studies for a number of years. Normalized Difference Vegetation Index (NDVI)[9], rather than single-channel data, are used due to the observed relationships between the index and vegetation productivity[10–13]. Data are 10-day (decadal) maximum-value composites to reduce the effects of cloudiness[14]. Most remaining noise in the time-series is negatively biased, however, some positively biased noise occurs, e.g. due to anisotropic effects, sensor problems etc[15]. Although efforts have been made to calibrate PAL data for sensor differences, geometry and atmospheric disturbances, quality problems remain[16]. The CLAVR cloud flag channel is used as a simple indicator of data quality. In CLAVR universal thresholds in all the five AVHRR channels are used to classify pixels as clear, mixed and cloudy[17]. CLAVR data has been shown to underestimate clear pixels[18]. Despite this deficiency the information can be used to improve NDVI estimates[19].

## 3. Methodology

We start by a general description of least-squares fits to an upper envelope. This is followed by an account on how to determine the number of annual seasons together with the approximate positions of their maxima and minima. The details of the adaptive Savitzky-Golay filter and the non-linear fitting to asymmetric Gaussians are given, and finally the extraction of seasonality information is discussed. The presented methods are implemented in a Fortran 90 program named TIMESAT and we refer to Jönsson and Eklundh[20,21] for computational aspects.

### 3.1. *Least-squares fits to an upper envelope*

Suppose that we have a time-series $(t_i, I_i)$, $i = 1, 2, ..., N$ and a model function $f(t)$ of the form

$$f(t) = c_1\varphi_1(t) + c_2\varphi_2(t) + \ldots + c_M\varphi_M(t), \tag{1}$$

where $\varphi_1(t), \varphi_2(t), \ldots, \varphi_M(t)$ are given basis functions. Then the best values, in the least-squares sense, of the parameters $c_1, c_2, \ldots, c_M$ are obtained as the solution of

the system of normal equations

$$\mathbf{A}^T\mathbf{A}\mathbf{c} = \mathbf{A}^T\mathbf{b}, \tag{2}$$

where

$$A_{ij} = \frac{\varphi_j(t_i)}{\sigma_i}, \qquad b_i = \frac{I_i}{\sigma_i}. \tag{3}$$

Here, $\sigma_i$ is the measurement uncertainty of the $i$th data point. If these are not known they may all be set to the constant value $\sigma = 1$. To estimate the uncertainty of the NDVI data points, the PAL cloud flag channel (CLAVR) can be used. There are no general rules as for how the cloud information should be transformed into uncertainty estimates and judicious settings are up to the user. For the runs over Africa presented in this paper the uncertainty parameters are set to 1.0, 1.5 or 100.0 for data values corresponding to the CLAVR classes clear, mixed and cloudy. To take into account the fact that most noise, even for data classified as clear by CLAVR, is negatively biased, the determination of the parameters $c_1, c_2, \ldots, c_N$ of the model function is done in two steps[20,21]. In the first step the parameters are obtained by solving the system of normal equations with $\sigma_i$ obtained from the ancillary data. Data points above the model function of the first fit are thought of as being more important, and in the second step the system is solved with the $\sigma_i$ of the high data points decreased by some factor. The multi-step procedure leads to a model function that is adapted to the upper envelope of the data (Figure 1).

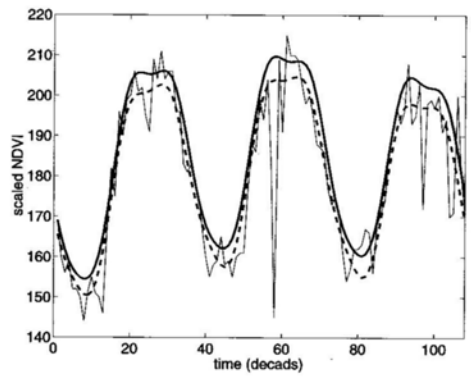


Fig. 1. Fitted functions from a two-step procedure. The dashed line shows a fitted function from the first step, and the solid line the fit from the second step.

### 3.2. *Determination of the number of seasons*

The high level of noise often makes it difficult to determine the number of annual seasons based on data for only one year. Including data from surrounding years

reduces the risk for erroneous determinations dramatically. In this work data values $(t_i, I_i)$, $i = 1, 2, ..., N$ for three years are fitted to a model function

$$f(t) = c_1 + c_2 t + c_3 t^2 + c_4 \sin(\omega t) + c_5 \cos(\omega t) + c_6 \sin(2\omega t) + c_7 \cos(2\omega t) + c_8 \sin(3\omega t) + c_9 \cos(3\omega t) \quad (4)$$

where $\omega = 6\pi/N$. With 10-day data used in this study $N = 108$. The first three basis functions determine the base level and the three-year trend whereas the three pairs of sine and cosine functions correspond to, respectively, one, two and three annual seasons. The fitting procedure always gives three primary maxima and minima. In addition, secondary and tertiary maxima and minima may be found. If the amplitude of the secondary maxima exceeds a certain fraction of the amplitude of the primary maxima, there are two annual seasons. If the amplitude of the secondary maxima is low the number of annual seasons is set to one. In Figure 2 (a) the primary maxima and minima dominate and the number of seasons is set to one. In Figure 2 (b) the secondary maxima and minima are comparatively large and the number of annual seasons is set to two.

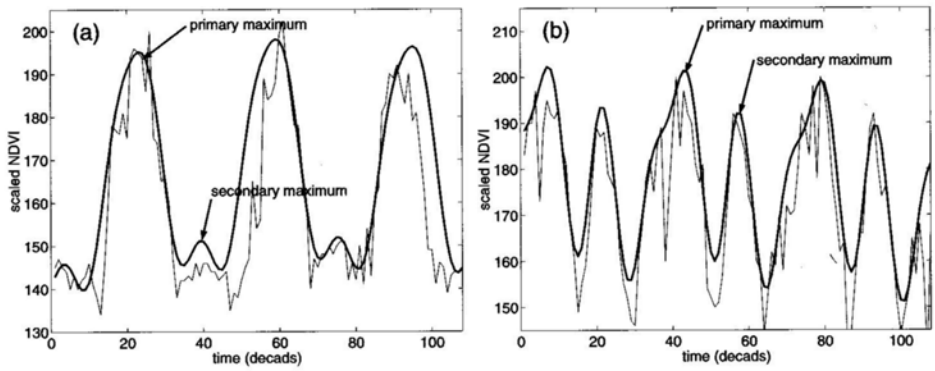


Fig. 2. Fits of sinusoidal functions and second order polynomials to three years of data in regions dominated by (a) one annual season and (b) two annual seasons. The thin solid line represents the original NDVI data. The thick solid line shows the fitted function.

### 3.3. *Locally adapted Savitzky-Golay filtering*

Savitzky-Golay filters are based on local polynomial fits[22]. For each point $i = 1, 2, \ldots, N$ a quadratic polynomial

$$f(t) = c_1 + c_2 t + c_3 t^2 \quad (5)$$

is fit to all $2n+1$ points in a window. The filtered value is then set to the polynomial value at this point. To account for the negatively biased noise, the fitting is done in multiple steps as described in the previous section. The result is a smoothed curve

that follows the upper envelope of the NDVI values. The width $n$ of the moving window determines the degree of smoothing, but it also affects the ability to follow a rapid change. In TIMESAT two values of $n$ can be set by the user. The first is used for data representing one annual season and the second for data representing two. Since, for large geographical areas, we are dealing with NDVI curves of different character it is desirable to use an adaptive method for $n$. Even if the global settings of the moving window work fairly well, it is sometimes necessary to locally tighten the window. A typical situation is in arid areas where the vegetation sometimes responds almost instantaneously to rainfall. To capture the corresponding sudden rise in data values, only a small window can be used. In TIMESAT the Savitzky-Golay filtering is performed using the global value $n$ of the window. The filtered data are then scanned and if there is a large increase or decrease in an interval around a data point $i$, this data point will be associated with a smaller window. The filtering is then redone with the new locally adapted sizes of the window. Savitzky-Golay filtering with and without the adaptive procedure is illustrated in Figure 3.

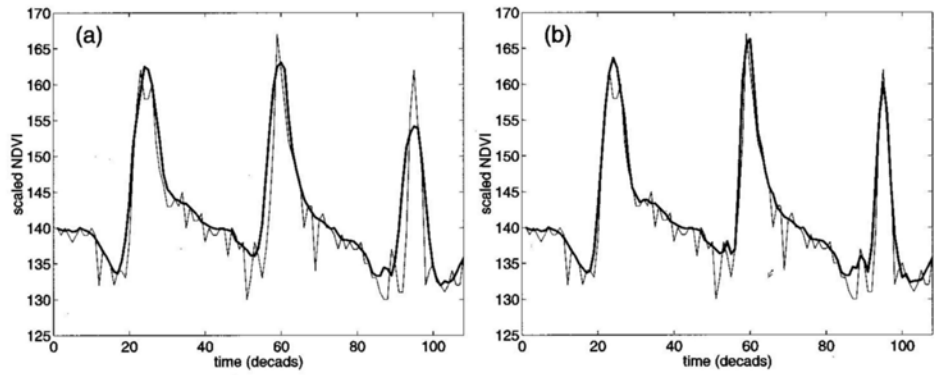


Fig. 3. Upper envelope Savitzky-Golay filtered data. Time is in ten day steps. In (a) the filtering is done with $n = 5$, which obviously is too large for the filtered data to follow the sudden increase and decrease of the underlying data values. A scan of the filtered data identifies the data points for which there is a large increase or decrease in surrounding intervals. Setting $n = 3$ for these points and redoing the filtering gives the curve in (b). Note the improved fit at the rising edges and at the narrow seasonal peaks.

### 3.4. *Least-squares fits to asymmetric Gaussian functions*

In the asymmetric Gaussian method local model functions

$$f(t) \equiv f(t; c_1, c_2, a_1, ..., a_5) = c_1 + c_2 g(t; a_1, ..., a_5), \tag{6}$$

are fitted to data in intervals around maxima and minima. Here

$$g(t; a_1, ..., a_5) = \begin{cases} \exp\left[-\left(\frac{t-a_1}{a_2}\right)^{a_3}\right] & \text{if } t > a_1 \\ \exp\left[-\left(\frac{a_1-t}{a_4}\right)^{a_5}\right] & \text{if } t < a_1 \end{cases} \tag{7}$$

is a Gaussian-type function. The linear parameters $c_1$ and $c_2$ determine the base level and the amplitude. For the Gaussian function, $a_1$ determines the position of the maximum or minimum with respect to the independent time variable $t$, while $a_2$ and $a_3$ determine the width and flatness (kurtosis) of the right function half. Similarly, $a_4$ and $a_5$ determine the width and flatness of the left half. The local model functions are well suited for describing the shape of the scaled NDVI time-series in overlapping intervals around maxima and minima. Given a set of data points in an interval $(t_i, I_i)$, $i = n_1, ..., n_2$ around a maximum or a minimum, the parameters $c_1$, $c_2$ and $a_1, ..., a_5$ are obtained by minimizing the merit function

$$\chi^2 = \sum_{i=n_1}^{n_2} \left[\frac{f(t_i; c_1, c_2, a_1, ..., a_5) - I_i}{\sigma_i}\right]^2. \tag{8}$$

The function depends non-linearly on the parameters $a_1, ..., a_5$ and in the program the minimization is done using an adaptive quasi-Newton method[23]. As in the previous cases the fitting is done in steps to account for the negatively biased noise. Given three local asymmetric Gaussian functions describing the left minimum, the central maximum and the right minimum (Figure 4 a), a global function fit can be built that describes the central season (Figure 4 b). The merging of local functions to a global function is a key feature of the method that increases the flexibility and allows the fitted function to follow a complex behavior of the time-series[20].

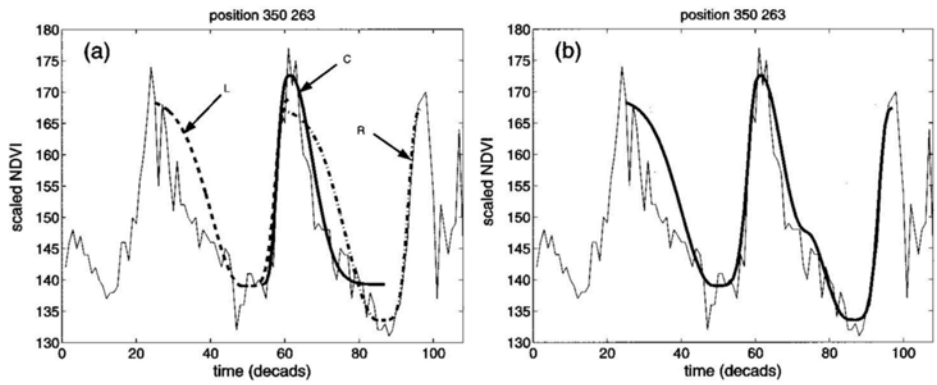


Fig. 4. (a) left (L), central (C) and right (R) local Gaussian functions. (b) merged global function. Note that the merged function in (b) only describes the vegetation of the central season from round decade 50 to decade 83. To describe vegetation of the left or right season additional local functions should be fitted and merged to global functions.

### 3.5. *Extraction of seasonality parameters*

Seasonal data are extracted for each of the growing seasons of the central year (Figure 5). Starting from the left base level or minimum, the beginning of a season is defined from the filtered or fitted functions as the point in time for which the value has risen by a certain amount, currently set to 10 % of the distance between the left base level and the maximum. The end of the season is defined in a similar way. The mid or the peak of a season is difficult to define, but a reasonable estimate is obtained as the position midway between the 90 % level positions above the left and right base levels. The annual integrated NDVI is frequently used in estimates of net primary production[25–27] through the relationship between NDVI and absorbed photosynthetically active radiation (APAR)[12]. To give a good estimate of the production of the phenologically dominant vegetation type it is also of interest to compute the integrated NDVI over the growing season, i.e. between the start and end of the season. In TIMESAT a small integral is defined as the area under the curve down to the mean of the left and right base levels. A large integral, extending to zero, is also defined.

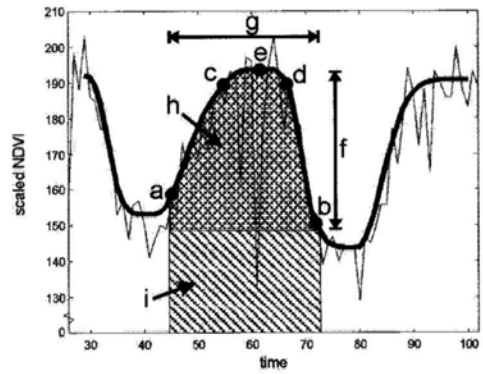


Fig. 5. Seasonality parameters computed in TIMESAT: (*a*) beginning of season, (*b*) end of season, (*c*) left 90 % level, (*d*) right 90 % level, (*e*) peak, (*f*) amplitude, (*g*) length of season, (*h*) integral over the growing season giving the area between the fitted function and the average of the left and right minimum values, (*i*) integral over the growing season giving the area between the fitted function and the zero level.

Other phenological parameters extracted are the peak values and the amplitude. The rate of increase in NDVI during the beginning of the season is theoretically related to the physiognomy of the vegetation and can be estimated by looking at the ratio between the amplitude and the time difference between the season start and the mid of the season. Another interesting quantity is the asymmetry, which can be defined as the ratio of the time differences between the mid of the season and the start and end of the season. A value of the asymmetry that is smaller than one indicate a rapid rise and a slow fall. Asymmetries larger than one, on the

other hand, are indicative of a slow rise and rapid fall. This type of behavior is often seen in areas with agricultural practices such as harvesting. Seasonal data can be extracted for single pixel locations and for whole images. Single pixel data are written to file and displayed with MATLAB. This is useful for testing the setting of parameters in specific locations. Image data are written to binary or ASCII files, and can be displayed with MATLAB or some suitable image processing software, like IDRISI, Easi/Pace or Erdas.

### 3.6. *Results*

We analyzed 1100 by 1060 pixels PAL image windows covering Africa over the period 1982-2000. For the sake of brevity, only a few examples are shown in this paper. These examples are selected to be representative of the differences between the two presented methods. Figure 6 shows the number of seasons, derived with the procedure outlined in Section 3.2. Areas characterized by two growing seasons (bi-modal) are mainly found in the Nile delta, parts of East Africa, along the Equator in central Africa, and in small areas along the coasts of West Africa. The sizes of these zones will vary somewhat with the parameter settings in the TIMESAT program. In Figure 6, pixels were classified as bi-modal if the amplitude of the secondary maxima were more than 40 % of the amplitude of the primary maxima. The observed pattern agrees well with what is expected given the general climatic circulation over Africa[28].

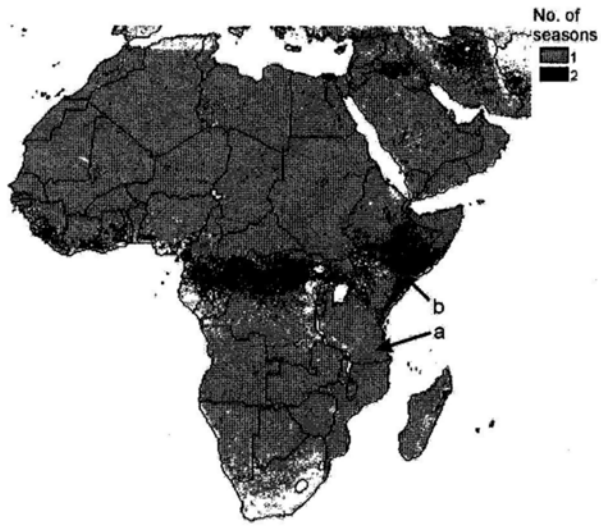


Fig. 6. Number of vegetational seasons in Africa 1999. Arrows point to uni-modal and bi-modal areas.

Figure 7 shows original NDVI and Savitzky-Golay filtered data for two areas, whose locations are indicated by the arrows in Figure 6. Figure 7 (a) is from a predominantly uni-modal (one season) area. Although there is a depression around the center of the central year, that might indicate the presence of two seasons, data is classified as uni-modal since the three years of data that have been used indicate that the area is dominated by a one seasonal cycle. Figure 7 (b), however, is bi-modal with two clearly developed growing cycles.

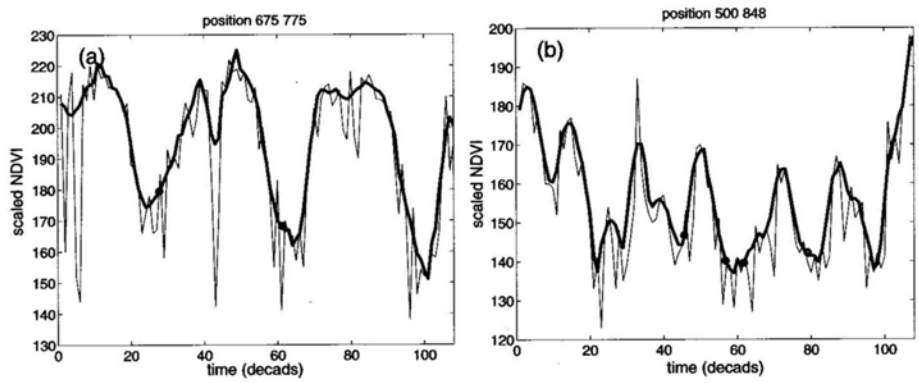


Fig. 7. NDVI and Savitzky-Golay filtered data from (a) uni-modal and (b) bi-modal areas, as indicated in Figure 7. Starts and ends of seasons are marked with circles.

Figure 8 displays original NDVI, Savitsky-Golay filtered data and asymmetric Gaussian functions for three pixels in Africa. The time-series in Figure 8 (a) is from the fringe of the Saharan desert, where the short annual season is dominated by a very rapid increase and decrease, followed by a slowly decreasing plateau. This composite behavior is typical for many extremely arid areas, and it is very well represented by the adaptive Savitzky-Golay method. However, the asymmetric Gaussian method has not represented the peak and the plateau of this time-series accurately. Figure 8 (b) is from a humid area with frequent cloudiness, resulting in a noisy time-series. The asymmetric Gaussian method has here generated a curve that is considerably smoother than the Savitzky-Golay filtered data. This smooth curve may be considered a better representative of the phenological curve of the vegetation, since some of the rapid changes seen in the Savitzky-Golay curve would not be expected to result from any physiological growth process, but rather from remaining noise due to clouds or other disturbances. Although the Savitzky-Golay curve follows the original data better, the smoothness of the asymmetric Gaussian curve might here be preferred. Figure 8 (c) was extracted from the Sahelian zone, well south of the Sahara. In this zone both the Savitzky-Golay and the asymmetric Gaussian function have modeled the time-series very well. Note that the beginnings and ends of seasons are located fairly close to each other in all three cases.

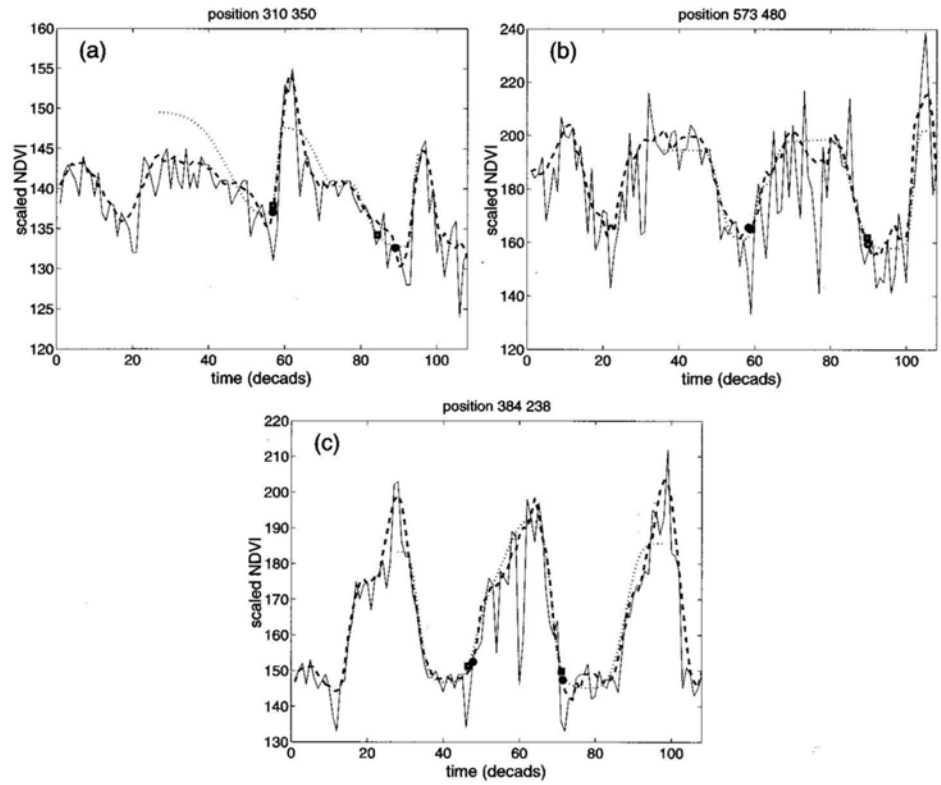


Fig. 8. Comparisons between Savitzky-Golay and asymmetric Gaussian curves for selected pixels. Beginnings and ends of seasons are marked by circles (Savitzky-Golay) and squares (asym. Gaussian). In (a) the Savitzky-Golay (dashed line) is superior to the asymmetric Gaussian (dotted line), which fails at following the rapid increase of the narrow central peak. In (b) the Gaussian method generates a smoother curve that better represents the behavior of vegetation than the curve generated by the Savitzky-Golay method. In (c) the both methods generate similar curves that both follow the data very well.

Figure 9 displays a number of parameters obtained with the Savitzky-Golay method. (a) gives the start of the first season in western Africa for 1999. Near the coast the season starts around decad 5 (end of February). The starting date then shifts towards later dates until the border of the Sahara, where it falls at about decad 25 (beginning of October). The observed pattern seems to be in general agreement with a climatic pattern dominated by the movements of the Inter Tropical Convergence Zone (ITCZ). In (b) the skewness or asymmetry is displayed. Note the belt with strong negative skewness that indicates a very rapid response to precipitation. (c) gives the peak value and (d) the amplitude for central Africa for the first growing season of 1999. In this area NDVI values are generally high. The seasonality of the evergreen vegetation, however, is not well developed and the resulting amplitudes are correspondingly small.

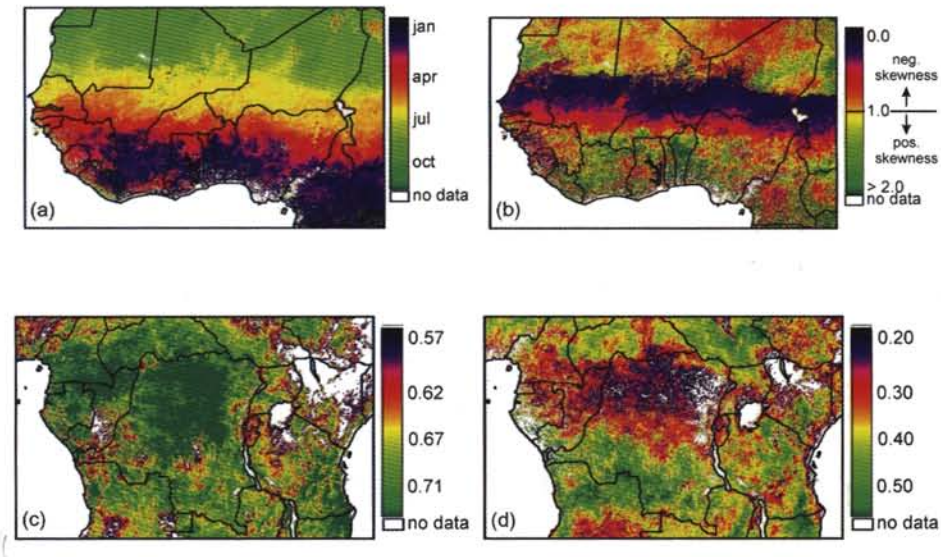


Fig. 9. Phenological parameters for the first growing season of 1999 extracted using Savitzky-Golay filtered data. (a) start of the growing season. (b) asymmetry or skewness. (c) peak value for the season. (d) amplitude of the season.

In order to investigate if there were any systematic differences between the two methods, values for some key phenological variables were extracted and averaged for each of the land-cover classes of the USGS digital land cover map[29,30]. Results for all classes, except those smaller than 5 % of the land area, are displayed in Table 1. The table indicates that the Savitzky-Golay method consistently generates higher values of amplitude and integrated NDVI than the asymmetric Gaussian method. Maximum values are also larger, but here the difference between the methods is smaller than for the other variables.

### 3.7. *Discussion*

Based on time-series of Pathfinder NDVI data the methods presented in this paper yield information about the seasonality of the underlying vegetation. Despite the high level of noise present in the original data the methods generate data that are spatially coherent and makes intuitive sense. AVHRR NDVI data are used in this study but other and newer sensor data are equally possible. The methods allow for ancillary data to be incorporated, and CLAVR cloudiness data is used as an indicator of uncertainties in the NDVI values. Although the effect of CLAVR was not explicitly tested, it is believed that new and better data quality indicators will improve the data fits. The seasonality patterns generated with the two

Table 1. Values for Savitzky-Golay (SG) and asymmetric Gaussian (AG) derived phenological variables computed as averages per USGS land cover class. Classes smaller than 5 % have been omitted.

| Class | Percentage of pixels | SG ampl. | AG ampl. | SG max. | AG max. | SG large integral | AG large integral | SG small integral | AG small integral |
|---|---|---|---|---|---|---|---|---|---|
| Dryland cropland and pasture | 5.9 | 45.2 | 39.2 | 187.3 | 186.1 | 5122.2 | 4681.2 | 821.7 | 709.9 |
| Grassland | 6.3 | 23.3 | 20.0 | 114.0 | 112.1 | 2991.0 | 2735.5 | 329.7 | 298.4 |
| Shrubland | 9.7 | 13.7 | 11.3 | 75.4 | 74.0 | 1483.7 | 1321.4 | 140.8 | 119.7 |
| Savanna | 25.8 | 47.4 | 41.3 | 191.5 | 190.4 | 5265.5 | 4841.1 | 843.5 | 740.4 |
| Evergreen broadleaf forest | 8.1 | 35.6 | 26.1 | 195.1 | 193.5 | 4853.9 | 4166.1 | 615.4 | 439.2 |
| Barren or sparsely vegetated | 32.4 | 0.6 | 0.5 | 3.3 | 3.2 | 85.3 | 75.8 | 9.9 | 8.3 |

methods largely correspond to each other with respect to the timings of seasonal events. However, some derived phenological parameters, notably the amplitude and the seasonal integrals, differ. The consistently lower values generated by the asymmetric Gaussian fits are believed to be underestimates due to the slower response to rapid phenological events. Although the timing of events is not much affected, amplitudes and integrals are. The possibility to modify the fits to handle these situations will have to be explored in future work. The asymmetric Gaussian functions generate smoother time-profiles that may represent the phenological behavior of vegetation better in some areas, notably when the time-series are very noisy. Thus, the two methods presented complement each other and the choice between them should be made based on the type of application and the behavior of the time-series in the specific area in mind. Other differences between the two methods are that the Savitzky-Golay algorithm is faster than the asymmetric Gaussian fit, and that it never fails to converge. This can happen with the non-linear Gaussian fit. However, of the 19 years of data over Africa analyzed, the asymmetric Gaussian fit only failed for a few hundred pixels, mostly over desert areas. The possibility to generate explicit information about the seasonality of the vegetation increases the potential use of time-series of satellite-derived spectral databases. It also underlines the importance of storing and maintaining long data series for the benefit of studies of phenological changes. Changes in key seasonality parameters might be used as early indicator of regional climatic changes.

## Acknowledgments

This work was supported by the Crafoord foundation. Lars Eklundh is employed on a grant from the Swedish National Space Board. Data used by the authors in this study include data produced through funding from the Earth Observing System Pathfinder Program of NASA's Mission to Planet Earth in cooperation with National Oceanic and Atmospheric Administration. The data were provided by Earth Observing System Data and Information System (EOSDIS), Distributed Active Archive Center at Goddard Space Flight Center which archives, manages, and distributes this data set.

## References

1. N. Viovy, O. Arino and A. S. Belward, *International Journal of Remote Sensing* **13**, 1585 (1992).
2. M. Menenti, S. Azzali, W. Verhoef and R. van Swol, *Advances in Space Research* **13**, 233 (1993).
3. L. Olsson and L. Eklundh, *International Journal of Remote Sensing* **15**, 3735 (1994).
4. J. Cihlar, *Remote Sensing of Environment* **56**, 149 (1996).
5. P. J. Sellers, C. J. Tucker, G. J. Collatz, S. O. Los, C. O. Justice, D. A. Dazlich and D. A. Randall, *International Journal of Remote Sensing* **15**, 3519 (1994).
6. G. J. Roerink, M. Menenti and W. Verhoef, *International Journal of Remote Sensing* **21**, 1911 (2000).

7. M. E. James and S. N. V. Kalluri, *International Journal of Remote Sensing* **15**, 3347 (1994).
8. J. R. G. Townshend, *International Journal of Remote Sensing* **15**, 3319 (1994).
9. J. W. J. Rouse, R. H. Haas, J. A. Schell and D. W. Deering, in *Third ERTS Symposium* (NASA SP-351, Washington DC, 1974), p. 309.
10. G. Asrar, M. Fuchs, E. T. Kanemasu and J. L. Hatfield, *Agronomy Journal* **76**, 300 (1984).
11. B. J. Choudhury, *Remote Sensing of Environment* **22**, 209 (1987).
12. C. J. Tucker and P. J. Sellers, *International Journal of Remote Sensing* **7**, 1395 (1986).
13. C. J. Tucker, C. Vanpraet, E. Boerwinkel and A. Gaston, *Remote Sensing of Environment* **13**, 461 (1983).
14. B. N. Holben, *International Journal of Remote Sensing* **7**, 1417 (1986).
15. G. G. Gutman, *Remote Sensing of Environment* **35**, 121 (1991).
16. S. D. Prince and S. N. Goward, *International Journal of Remote Sensing* **17**, 217 (1996).
17. L. L. Stowe, E. P. McClain, R. Carey, P. Pellegrino, G. Gutman, P. Davis, C. Long and S. Hart, *Advances in Space Research* **3**, 51 (1991).
18. S. Vemury, L. L. Stowe and V. R. Anne, *Journal of Atmospheric and Oceanic Technology* **18**, 169 (2001).
19. G. Gutman and A. Ignatov, *International Journal of Remote Sensing* **17**, 3295 (1996).
20. P. Jönsson and L. Eklundh, *IEEE Transactions on Geoscience and Remote Sensing* **40**, 1824 (2002).
21. P. Jönsson and L. Eklundh, *Computers and Geosciences*, (in preparation).
22. W. H. Press, S. A. Teukolsky, W. T. Vetterling and B. P. Flannery, *Numerical Recipes in FORTRAN. The art of scientific computing, Second edition*, (Cambridge University Press, Cambridge, 1992), p. 963.
23. J. E. Dennis, D. M. Gay and R. E. Welsch, *ACM Transactions on Mathematical Software* **7**, 348 (1981).
24. C. B. Field, M. J. Behrenfeld, J. T. Randerson and P. Falkowski, *Science* **281** 237 (1998).
25. A. Ruimy, B. Saugier and G. Dedieu, *Journal of Geophysical Research* **99**, 5263 (1994).
26. S. W. Running and R. R. Nemani, *Remote Sensing of Environment* **24**, 347 (1988).
27. S. N. Goward and D. G. Dye, *Advances in Space Research* **7**, 165 (1987).
28. H. E. Landsberg, *Climates of Africa. World Survey of Climatology*, (Elsevier, Amsterdam, 1972).
29. USGS/NASA, Africa Land Cover Characteristics Data Base Ver. 2.0. Internet reference: URL: `http://edcdaac.usgs.gov/glcc/afdoc2_0.html`. Accessed on 14 Aug. 2002, 2002.
30. T. R. Loveland, Z. Zhu, D. O. Ohlen, J. F. Brown, B. C. Reed and L. Yang, *Photogrammetric Engineering and Remote Sensing* **65**, 1021 (1999).